

Interacting topological magnons in the Kitaev-Heisenberg honeycomb ferromagnet with the Dzyaloshinskii-Moriya interaction

Jie Wang, Jin Wen Li, Pei Chen, Bing Tang*

Department of Physics, Jishou University, Jishou 416000, China

ABSTRACT

The study of the Heisenberg-Kitaev honeycomb ferromagnets has recently drawn attention because of their rich topological properties. Topological phase transitions may arise when there exist two or more distinct topological phases, and they are often revealed by a gap-closing phenomenon. In this work, we investigate the magnonic properties of honeycomb ferromagnets exhibiting Kitaev and DMI interactions in the presence of a Heisenberg exchange and magnetocrystalline anisotropy exposed to a magnetic field. We employ the Self-Consistent Renormalization (SCR) spin wave theory to investigate the effects of magnon-magnon interactions (MMIs) and thermal fluctuations on the properties of magnons. Our findings demonstrate that the magnon system undergoes topological phase transitions driven by temperature and magnetic fields, which are attributed to MMIs. Specifically, as the temperature rises, the magnon band gap at the Dirac points closes and reopens at the critical temperature T_c , which is below the Curie temperature. By showing that the Chern numbers of the magnonic bands are distinct above and below T_c , we confirm that the gap-closing phenomenon is indeed a signature for the topological phase transitions. Furthermore, our analysis indicates that the thermal Hall conductivity in the magnonic system exhibits a sign reversal at T_c , which can serve as an experimental probe of its

* Corresponding author.

E-mail addresses: bingtangphy@jsu.edu.cn

topological nature.

I. INTRODUCTION

The last 20 years have witnessed the extraordinary development of topological insulators and semimetals in the field of condensed matter physics [1-6]. In analogy to electronic systems, the topological phases have also been extended to bosonic systems, such as photonic and magnons [6-9].

Magnons, which are quantized spin excitations in magnets and bosons, have also been proposed to host nontrivial topological phases [10-20]. As fundamental excitation modes in magnetic systems, they can be well described by linear spin wave theory at zero temperature. The topology of Heisenberg-Kitaev honeycomb ferromagnets has also been discussed in linear spin wave theory in some works [10-13]. For example, Joshi *et al.* [47] show that the topological phase transition can be tuned by applying an external magnetic field or by making the Kitaev couplings anisotropic. Zhang *et al.* [48] have investigated the magnonic properties of honeycomb ferromagnets with DMI and Kitaev interaction subject to an external magnetic field. The possibility of achieving magnon topological phase states above a finite temperature is seldom proposed. However, at finite temperatures, magnon interactions become significant, and linear theory fails to capture these interactions. Therefore, considering the interplay between spin wave interactions and thermal fluctuations is indispensable for understanding the complex dynamics within magnetic systems [21-40].

Recent research has provided new insights into the nonlinear characteristics of magnon behavior and topological phase transitions in magnetic systems [39-41]. Such as, Zhu *et al.* [39] have found that in checkerboard ferromagnets, interactions between magnons, particularly the antichiral DMI, can cause changes in the magnon band gap near the Dirac point with temperature variations, thereby inducing topological phase transitions. Additionally, Li *et al.* [41] focused on collinear antiferromagnets, especially the two-dimensional material MnPS_3 , and discovered through

self-consistent renormalization spin wave theory that an increase in temperature can induce the formation of topological magnon Chern insulators. These findings not only deepen our understanding of magnon topological phase transitions but also provide a theoretical foundation for new topological phases and potential applications in magnetic materials.

In this paper, we show that increasing temperature can induce a topological phase transition for magnons by considering the two-dimensional Heisenberg-Kitaev honeycomb ferromagnet as the research object. By employing the SCR spin wave theory, we systematically analyze the effects of magnon-magnon interactions and thermal fluctuations on the properties of magnons in the Heisenberg-Kitaev honeycomb ferromagnet. We focus on systems with Kitaev and DMI interactions, influenced by Heisenberg exchange, magnetocrystalline anisotropy, and an external magnetic field. We use finite-temperature field theory to handle many-body interactions. First, we calculated the magnetization at finite temperatures using the SCR spin wave theory, which enhanced the reliability of the theoretical framework crucial for understanding the interplay between external conditions and the system's response. Next, we calculated the magnon bands and corresponding topological invariants at finite temperatures and low magnetic fields, discussing topological phase transitions triggered by temperature increases and magnetic field changes. Additionally, we examined the thermal Hall effect, finding that the closing and reopening of the band gap are accompanied by a magnon chirality switch and a non-trivial Berry curvature transition near the \mathbf{K} point. These phenomena can be explored in actual experiments. Our theoretical study has provided a comprehensive numerical analysis and has proposed the possibility of achieving magnon topological phase states above a finite temperature T_c .

II. Model

We consider an extended ferromagnetic Kitaev-Heisenberg model on the honeycomb lattice, which includes DMI and a single-ion anisotropy term in a uniform magnetic field \vec{B} . The spin Hamiltonian is given by

$$\mathcal{H} = J \sum_{\langle i,j \rangle} \mathbf{S}_i \cdot \mathbf{S}_j + 2K \sum_{\langle\langle i,j \rangle\rangle} S_i^\gamma S_j^\gamma + \sum_{\langle\langle ij \rangle\rangle} \mathbf{D}_{ij} \cdot (\mathbf{S}_i \times \mathbf{S}_j) - \sum_i A (\mathbf{e}_z \cdot \mathbf{S}_i)^2 - \mu_B g B \mathbf{e}_z \cdot \sum_i \mathbf{S}_i, \quad (1)$$

where, the first and second terms denote the first-nearest-neighbor Heisenberg ferromagnetic exchange interaction and the bond-dependent Kitaev coupling interaction, respectively. The index $\gamma \in \{X, Y, Z\}$ stands for the bond form as depicted in Fig. 1. These two interactions can be parameterized as $J = R \cos \theta$ and $K = R \sin \theta$, where $\theta \in [0, 2\pi]$ and $R = \sqrt{J^2 + K^2} > 0$ is the overall energy scale. The third term corresponds to the antisymmetric DMI of the second nearest neighbors. $\mathbf{D}_{ij} = D v_{ij} \mathbf{e}_z$ is the DMI vector, and the coefficient $v_{ij} = -v_{ji} = \pm 1$ depends on the orientation of the two second-nearest-neighbor spins. Additionally, as a larger θ enhances the effect of the anisotropic exchange interaction, we add a single-ion anisotropy term with respect to the local easy axis \mathbf{e}_z to ensure the stability of the system. And the energy of Zeeman coupling to the magnetic field B . We define $h \equiv \mu_B g B$, where g is the g -factor and μ_B is the Bohr magneton, where \mathbf{e}_z is applied parallel to [111], as displayed in Fig. 1.

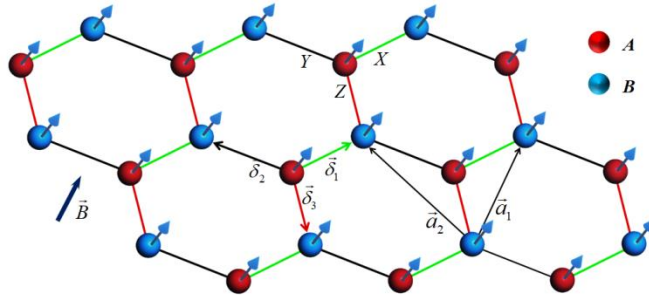


FIG. 1. Illustration of the Kitaev-Heisenberg honeycomb ferromagnetic lattice. With bond links $\gamma \in \{X, Y, Z\}$ for the Kitaev interaction in Eq. (1). The primitive lattice

vectors are $\mathbf{a} = \left(\pm \frac{\sqrt{3}}{2}, \frac{3}{2} \right) a$ and the nearest-neighbour vectors are $\boldsymbol{\delta}_1 = \left(\frac{\sqrt{3}}{2}, \frac{1}{2} \right) a$, $\boldsymbol{\delta}_2 = \left(\frac{\sqrt{3}}{2}, \frac{1}{2} \right) a$, $\boldsymbol{\delta}_3 = (0, -1) a$. Here, A and B denote the two sublattices of the honeycomb lattice.

We now incorporate the Holstein-Primakoff transformation [13] to recast spin operators in terms of deviation creation (a_i^+) and annihilation (a_i) operators, streamlining our analysis of spin dynamics, $S_i^z = S - a_i^+ a_i$, $S_i^+ = \sqrt{2S - a_i^+ a_i} a_i$, $S_i^- = a_i^+ \sqrt{2S - a_i^+ a_i}$, for the A-sublattice (similarly for the B-sublattice). In this work, going beyond LSWT, we consider RSWT. We substitute the form of the second-order expansion using the HP transformation into Eq. (1), keeping the terms up to quartic order and neglecting the ground state energy term. Next, we separate the total Hamiltonian \mathcal{H} into two terms. $\mathcal{H} = \mathcal{H}^{(2)} + \mathcal{H}^{(4)}$. Then, we apply the Fourier transform to the magnon operators, that the two-particle term can be written in the form $\mathcal{H}^{(2)} = \frac{1}{2} \sum_{\mathbf{k}} \psi_{\mathbf{k}}^+ H_0(\mathbf{k}) \psi_{\mathbf{k}}$, where $\psi_{\mathbf{k}} = (a_{\mathbf{k}}, b_{\mathbf{k}}, a_{-\mathbf{k}}^+, b_{-\mathbf{k}}^+)^T$. The third and fourth columns represent the hole states with a negative energy spectrum (non-physical).

We analyze the band structure in the following section. The Hamiltonian matrix $H_{\mathbf{k}}$ are given by

$$H_0(\mathbf{k}) = \begin{pmatrix} M_{\mathbf{k}} & B_{\mathbf{k}} \\ [B_{\mathbf{k}}]^\dagger & [M_{-\mathbf{k}}]^T \end{pmatrix}, \quad (2)$$

with

$$M_{\mathbf{k}} = \begin{pmatrix} h_A & m_{\mathbf{k}} \\ m_{\mathbf{k}}^* & h_B \end{pmatrix}, \quad B_{\mathbf{k}} = \begin{pmatrix} 0 & \rho_{\mathbf{k}} \\ \rho_{-\mathbf{k}} & 0 \end{pmatrix}, \quad (3)$$

where $h_{B/A} = -3S(J_H + \frac{2}{3}J_K) + A(2S - 1) + h \pm \frac{2S}{3} Dd_{\mathbf{k}}$, $m_{\mathbf{k}} = f_{\mathbf{k}}(J_H + \frac{2}{3}J_K)$,

$$\rho_{\mathbf{k}} = \frac{2}{3} g_{\mathbf{k}} J_K \quad , \quad f_{\mathbf{k}} = (1 + e^{i\mathbf{k}\cdot\mathbf{a}_1} + e^{i\mathbf{k}\cdot\mathbf{a}_2}) \quad , \quad g_{\mathbf{k}} = (1 + e^{i(\mathbf{k}\cdot\mathbf{a}_1 - 2\pi/3)} + e^{i(\mathbf{k}\cdot\mathbf{a}_2 + 2\pi/3)}) \quad , \quad \text{and}$$

$$d_{\mathbf{k}} = \sum_{n=1}^3 (\sin(\mathbf{k}\cdot\boldsymbol{\zeta}_n)) .$$

We now discuss the nonlinear part. In lattice-space representation, the four-particle term $\mathcal{H}^{(4)}$ reads :

$$\begin{aligned} \mathcal{H}^{(4)} = \frac{1}{N} \sum_{\{\mathbf{k}_i\}} & \left\{ -(J_H + \frac{2}{3} J_K) \frac{1}{4} (f_{\mathbf{k}_4} a_{\mathbf{k}_1}^+ a_{\mathbf{k}_2}^+ a_{\mathbf{k}_3} b_{\mathbf{k}_4} + f_{\mathbf{k}_4} b_{\mathbf{k}_1} b_{\mathbf{k}_2}^+ b_{\mathbf{k}_3}^+ a_{\mathbf{k}_4} - 4 f_{\mathbf{k}_4 - \mathbf{k}_2} a_{\mathbf{k}_1}^+ b_{\mathbf{k}_2}^+ a_{\mathbf{k}_3} b_{\mathbf{k}_4} \right. \\ & + H.c) \delta_{\{\mathbf{k}_i\}}^1 - \frac{J_K}{6} (g_{\mathbf{k}_4} b_{\mathbf{k}_1} b_{\mathbf{k}_2}^+ b_{\mathbf{k}_3}^+ a_{\mathbf{k}_4}^+ + g_{-\mathbf{k}_4} a_{\mathbf{k}_1} a_{\mathbf{k}_2}^+ a_{\mathbf{k}_3}^+ b_{\mathbf{k}_4}^+ + H.c) \delta_{\{\mathbf{k}_i\}}^2 \\ & \left. + [(\Pi_D - A) a_{\mathbf{k}_1}^+ a_{\mathbf{k}_2}^+ a_{\mathbf{k}_3} a_{\mathbf{k}_4} + (-\Pi_D - A) \rho b_{\mathbf{k}_1}^+ b_{\mathbf{k}_2}^+ b_{\mathbf{k}_3} b_{\mathbf{k}_4}] \delta_{\{\mathbf{k}_i\}}^1 \right\} \end{aligned} \quad , \quad (7)$$

where $\delta_{\{\mathbf{k}_i\}}^1 = \delta_{\mathbf{k}_1 + \mathbf{k}_2, \mathbf{k}_3 + \mathbf{k}_4}$, $\delta_{\{\mathbf{k}_i\}}^2 = \delta_{\mathbf{k}_1, \mathbf{k}_2 + \mathbf{k}_3 + \mathbf{k}_4}$ and $\Pi_D = \frac{D}{6N} (d_{\mathbf{k}_2} + d_{\mathbf{k}_4})$.

We now have a spin Hamiltonian with a non-interacting part $\mathcal{H}^{(2)}$ and an interacting part $\mathcal{H}^{(4)}$. In the context of examining the interplay between many-body effects and thermal fluctuations, we utilize the Green's function approach. Specifically, we define a matrix Green's function as $\mathcal{G}(\mathbf{k}, \tau) = -\langle \mathcal{T}_\tau \psi_{\mathbf{k}}(\tau) \psi_{\mathbf{k}}^+(0) \rangle$, where \mathcal{T}_τ represents the time-ordering operator in imaginary time $\tau = it$, and $0 \leq \tau \leq \beta$ with $\beta = (k_B T)^{-1}$. The τ -dependent operator is defined as $O(\tau) = e^{\mathcal{H}\tau} O(0) e^{-\mathcal{H}\tau}$, which is formally obtained by the analytic continuation to imaginary time τ of the Heisenberg operator $O(t)$, and $\mathcal{H} = \mathcal{H}_0 + \mathcal{H}_{\text{int}}$ is the effective Hamiltonian. The bracket $\langle \dots \rangle$ denotes the thermodynamic average. To solve for the Green's function elements, we address the Heisenberg equation of motion and apply the random phase approximation to extract nonlinear self-energy corrections arising from many-body interactions (MMIs), The Green's function is given by

$$\begin{aligned}\frac{d\mathcal{G}(\mathbf{k}, \tau)}{d\tau} &= -\delta(\tau)\tau_z - \langle \mathcal{T}_\tau [\mathcal{H}, \psi_{\mathbf{k}}(\tau)] \psi_{\mathbf{k}}^+(0) \rangle \\ &= -\delta(\tau)\tau_z - \tau_z (H_0 + \sum_{\mathbf{k}}) \mathcal{G}(\mathbf{k}, \tau)\end{aligned}\quad (8)$$

Here the self-energy term $\sum_{\mathbf{k}}$ is from the random phase approximation.

Subsequently, we perform a Fourier transformation to obtain the desired

frequency-domain representation. $\mathcal{G}(\mathbf{k}, \tau) = \frac{1}{\beta} \sum_n e^{-i\omega_n \tau} \mathcal{G}(\mathbf{k}, \omega_n) e^{-i\omega_n \tau}$, $\beta = 1/T$ where

T is the temperature, with ω_n representing the bosonic Matsubara frequency.

Through these steps, we can get $-i\omega_n \mathcal{G}(\mathbf{k}, \omega_n) = -\tau_z - \tau_z H_1(\mathbf{k}) \mathcal{G}(\mathbf{k}, \omega_n)$, By

multiplying both sides by the τ_z term, we can obtain the Dyson's equation

$\mathcal{G}^{-1}(\mathbf{k}, \omega_n) = i\omega_n \tau_z - H_1(\mathbf{k})$ and the effective Hamiltonian. Here, \mathcal{G}^{-1} is the inverse

of the Green's function, and $H_{\mathbf{k}}^{eff} = H_{\mathbf{k}} + \sum_{\mathbf{k}}$ is the renormalized effective

Hamiltonian:

$$H_{\mathbf{k}}^{eff} = \begin{pmatrix} M_{\mathbf{k}}^{eff} & B_{\mathbf{k}}^{eff} \\ [B_{\mathbf{k}}^{eff}]^\dagger & [M_{-\mathbf{k}}^{eff}]^T \end{pmatrix}, \quad (9)$$

with

$$M_{\mathbf{k}}^{eff} = \begin{pmatrix} h_A^{eff} & m_{\mathbf{k}}^{eff} \\ (m_{-\mathbf{k}}^{eff})^* & h_B^{eff} \end{pmatrix}, \quad B_{\mathbf{k}}^{eff} = \begin{pmatrix} 0 & \rho_{\mathbf{k}}^{eff} \\ \rho_{-\mathbf{k}}^{eff} & 0 \end{pmatrix}, \quad (10)$$

where

$$h_A^{eff} = -3J_0 \bar{S}_B - \frac{2D}{3} d_{\mathbf{k}} \bar{S}_A + h_{a,b} + A(-2S - 1 + 4\bar{S}_A), \quad (11)$$

$$h_B^{eff} = -3J_0 \bar{S}_A + \frac{2D}{3} d_{\mathbf{k}} \bar{S}_B + h_{a,b} + A(-2S - 1 + 4\bar{S}_B), \quad (12)$$

$$m_{\mathbf{k}}^{eff} = \frac{J_0}{2} (\bar{S}_A + \bar{S}_B) f_{\mathbf{k}} + \frac{J_0}{N} \sum_q f_{\mathbf{k}-\mathbf{q}} \langle b_{\mathbf{q}}^+ a_{\mathbf{q}} \rangle, \quad (13)$$

$$\rho_{\mathbf{k}}^{eff} = \frac{1}{3} J_K g_{\mathbf{k}} (\bar{S}_A + \bar{S}_B) + J_0 \frac{1}{N} \sum_q f_{\mathbf{k}-\mathbf{q}} \langle a_{\mathbf{q}} b_{-\mathbf{q}} \rangle, \quad (14)$$

$$J_0 = J + 2K/3, \quad \bar{S}_A = S - \frac{1}{N} \sum_{\mathbf{q}} \langle a_{\mathbf{q}}^+ a_{\mathbf{q}} \rangle, \quad \bar{S}_B = S - \frac{1}{N} \sum_{\mathbf{q}} \langle b_{\mathbf{q}}^+ b_{\mathbf{q}} \rangle, \quad (15)$$

$$h_{a,b} = -\frac{J_0}{N} \sum_{\mathbf{q}} \text{Re} \left(f_{\mathbf{q}} \langle a_{\mathbf{q}}^+ b_{\mathbf{q}} \rangle \right) - \frac{2J_K}{3N} \sum_{\mathbf{q}} \text{Re} \left(g_{\mathbf{q}} \langle a_{\mathbf{q}}^+ b_{-\mathbf{q}}^+ \rangle \right) + h, \quad (16)$$

In the random phase approximation method, other terms are always zero and are therefore neglected. The quadratic bosonic Hamiltonian $H_{\mathbf{k}}$ can be diagonalized via a standard canonical Bogoliubov transformation. We need to find a transformation matrix $\Lambda_{\mathbf{k}}$ from a new basis $\phi_{\mathbf{k}}$ to the old basis: $\psi_{\mathbf{k}} = \Lambda_{\mathbf{k}} \phi_{\mathbf{k}}$, where $\phi_{\mathbf{k}} = (\alpha_{\mathbf{k}}, \beta_{\mathbf{k}}, \alpha_{-\mathbf{k}}^+, \beta_{-\mathbf{k}}^+)^T$ are the Bogoliubov quasiparticles, \mathbf{k} is the magnon wavevector, and $\Lambda_{\mathbf{k}}$ is a 4×4 paraunitary matrix, which ensures the preservation of the commutation relations in the transformed basis. The paraunitary matrix $\Lambda_{\mathbf{k}}$ satisfies the following relation: $\Lambda_{\mathbf{k}}^\dagger \tau_z \Lambda_{\mathbf{k}} = \tau_z$, and τ_z is the Pauli matrix that preserves certain symmetries or properties of the physical system in the Bogoliubov transformation. This approach is essential for understanding the behavior of magnons in the system, especially when considering the effects of nonlinear interactions and temperature-induced changes.

From the diagonalization matrix $T_{\mathbf{k}}$, we have the relations:

$$a_{\mathbf{k}} = u_{\mathbf{k},a,\alpha} \alpha_{\mathbf{k}} + u_{\mathbf{k},a,\beta} \beta_{\mathbf{k}} + v_{-\mathbf{k},a,\alpha} \alpha_{-\mathbf{k}}^+ + v_{-\mathbf{k},a,\beta} \beta_{-\mathbf{k}}^+, \quad (17)$$

$$b_{\mathbf{k}} = u_{\mathbf{k},b,\alpha} \alpha_{\mathbf{k}} + u_{\mathbf{k},b,\beta} \beta_{\mathbf{k}} + v_{-\mathbf{k},b,\alpha} \alpha_{-\mathbf{k}}^+ + v_{-\mathbf{k},b,\beta} \beta_{-\mathbf{k}}^+, \quad (18)$$

After a change of basis, the thermal averages can be expressed in terms of the parameters and, as well as the occupation number of the bands. For example:

$$\begin{aligned} \sum_{\mathbf{q}} \langle a_{\mathbf{q}}^+ a_{\mathbf{q}} \rangle &= \frac{1}{N} \sum_{\mathbf{q}} \left(|u_{\mathbf{q},a,\alpha}|^2 \langle \alpha_{\mathbf{q}}^+ \alpha_{\mathbf{q}} \rangle + |u_{\mathbf{q},a,\beta}|^2 \langle \beta_{\mathbf{q}}^+ \beta_{\mathbf{q}} \rangle + |v_{-\mathbf{q},a,\alpha}|^2 \langle \alpha_{-\mathbf{q}} \alpha_{-\mathbf{q}}^+ \rangle + |v_{-\mathbf{q},a,\beta}|^2 \langle \beta_{-\mathbf{q}} \beta_{-\mathbf{q}}^+ \rangle \right) \\ &= \frac{1}{N} \sum_{\mathbf{q}} \left(|u_{\mathbf{q},a,\alpha}|^2 n_{\mathbf{q},\alpha} + |u_{\mathbf{q},a,\beta}|^2 n_{\mathbf{q},\beta} + |v_{-\mathbf{q},a,\alpha}|^2 (1+n_{-\mathbf{q},\alpha}) + |v_{-\mathbf{q},a,\beta}|^2 (1+n_{-\mathbf{q},\beta}) \right) \\ &= \sum_{\mathbf{q},\lambda=\alpha,\beta} \left(|u_{\mathbf{q},a,\lambda}|^2 + |v_{\mathbf{q},a,\lambda}|^2 \right) n_{\mathbf{q},\lambda} + |v_{\mathbf{q},a,\lambda}|^2 \\ \sum_{\mathbf{q}} \langle b_{\mathbf{q}}^+ b_{\mathbf{q}} \rangle &= \sum_{\mathbf{q},\lambda=\alpha,\beta} \left(|u_{\mathbf{q},b,\lambda}|^2 + |v_{\mathbf{q},b,\lambda}|^2 \right) n_{\mathbf{q},\lambda} + |v_{\mathbf{q},b,\lambda}|^2 \end{aligned} \quad (19)$$

The element of the self-energy matrix can be expressed as:

$$\sum_{\mathbf{k}}^{ij} = \frac{1}{N} \sum_{\mathbf{q}, \lambda=\alpha, \beta} [T_{ij}^{\lambda}(\mathbf{k}, \mathbf{q}) n_{\mathbf{q}, \lambda}(T) + Q_{ij}^{\lambda}(\mathbf{k}, \mathbf{q})] . \quad (20)$$

Here, $n_{\mathbf{q}, \lambda}$ denotes the Bose-Einstein distribution function, given by $n_{\mathbf{q}, \alpha} = \langle \alpha_{\mathbf{q}}^+ \alpha_{\mathbf{q}} \rangle = (e^{E_{\mathbf{q}}^{\alpha}/T} - 1)^{-1}$, $n_{\mathbf{q}, \beta} = \langle \beta_{\mathbf{q}}^+ \beta_{\mathbf{q}} \rangle = (e^{E_{\mathbf{q}}^{\beta}/T} - 1)^{-1}$. The terms $\langle \alpha_{\mathbf{q}}^+ \alpha_{\mathbf{q}} \rangle$ and $\langle \beta_{\mathbf{q}}^+ \beta_{\mathbf{q}} \rangle$ are the only non-zero thermal averages in the new foundation. The last two terms in Eq. (20) account for the thermal and quantum corrections, respectively, with the self-energy corrections persisting even at zero temperature due to quantum fluctuations. Consistent with previous studies [38,39], Eq. (9) and (20), along with the mentioned diagonalization relationship, establish the self-consistent equations. Using these equations, we can determine the band structures and magnetization at specific temperatures in a self-consistent manner and derive the corresponding Chern numbers.

III. RESULTS AND DISCUSSIONS

In ferromagnets, the Curie temperature is the threshold at which materials shift from a ferromagnetic to a paramagnetic state. In this study, $\bar{S} = \bar{S}_A = \bar{S}_B$ serves as the order parameter characterizing the magnetic phase transition. The total magnetization along the \mathbf{z} direction is defined as $\langle S_z \rangle = S - \frac{1}{N} \sum_{\mathbf{q}} \langle a_{\mathbf{q}}^+ a_{\mathbf{q}} \rangle$. We first determine the Curie temperature by self-consistently solving for the magnetization intensity, ensuring the validity of our theoretical framework. In fig. 2(b) illustrates the effects of the magnetic field and temperature on the magnetic susceptibility. The black solid line represents the boundary where the magnetization intensity is below 0.1. Through this phase diagram, we can intuitively observe that an increase in the magnetic field leads to an elevation of the Curie temperature. This confirms that the magnetic field enhances magnetic anisotropy and suppresses spin fluctuations. Similarly, in Fig. 2(b), the effects of the DMI strength on the magnetization intensity are shown. By comparison, we can see that at higher temperatures, DMI has almost no effect on the magnetization intensity.

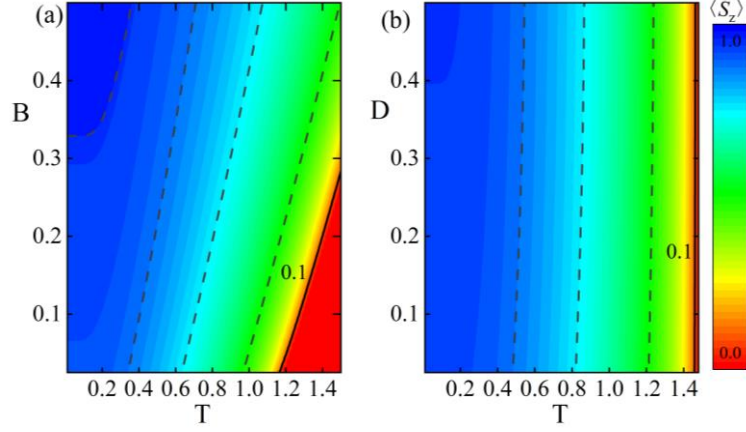


FIG. 2. (a) The total magnetization distribution in the $T-B$ plane. The solid black line segments represent the boundary where the magnetic susceptibility is zero. To the right of the solid lines is the forbidden region. The other parameters are adopted as $S=1$ $R=1$ $D=0.28$ $\theta=1.45$. In subsequent calculations, we adopt the same parameters when not stated otherwise. (b) The total magnetization distribution in the $D-B$ plane, $h=0.25$.

Based on the above, we have verified that the magnitude of the DMI has little effect on the distribution of magnetic susceptibility. Therefore, we continue to analyze the competitive relationship between spin fluctuations induced by temperature and the anisotropy energy enhanced by the magnetic field, under various strengths of the DM interaction.

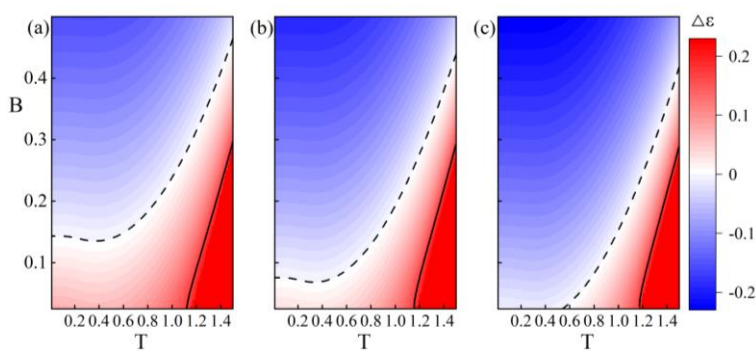


FIG. 3. Band gap Δ_K as a function of T and B at $D=0.27;0.28;0.29$. The dashed black line represents the condition where the band gap difference at the \mathbf{K} point is zero. The solid black line marks the boundary where magnetization is about 0.1.

Both the DMI and Kitaev interaction are capable of altering the magnon dispersion relations and opening an energy gap at the \mathbf{K} point. By fine-tuning the magnitudes of the DMI and Kitaev parameters, it is possible to achieve the same energy gap size at the \mathbf{K} point through various combinations. Furthermore, we have discovered that adjusting the temperature and magnetic field strength can also result in energy gaps of different sizes. To further compare the impact of this competition on the energy gap, we have constructed phase diagrams illustrating the dependence of the energy difference at the \mathbf{K} point on temperature and magnetic field strength, as shown in Fig. 3. We found that within a certain temperature range, it is possible to achieve the closure and opening of energy bands by adjusting the magnetic field strength and temperature.

To suppress spin fluctuations, we chose a magnetic field strength of 0.25 and studied the variation of the band gap difference at the \mathbf{K} point with DMI strength at different temperatures below the Curie temperature, as shown in Fig. 4.

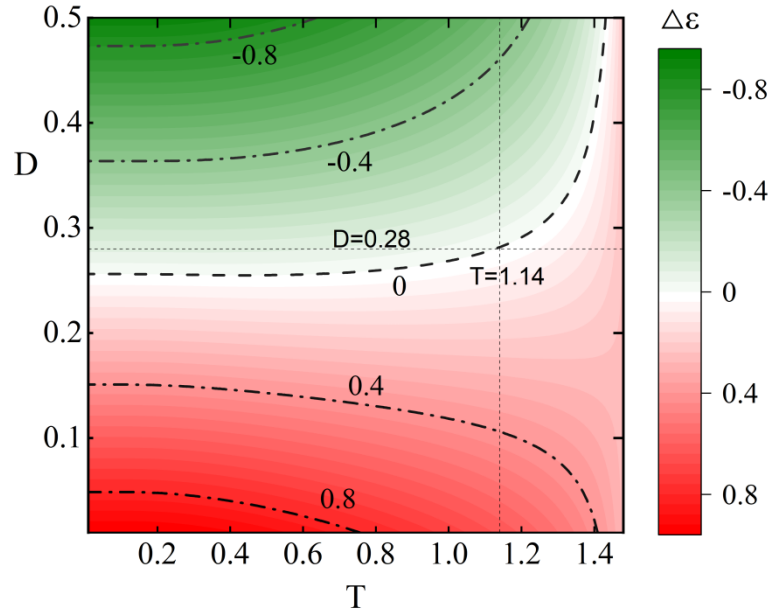


FIG. 4 Band gap Δ_K as a function of T and D at $B = 0.25$.

To more intuitively present the topological transitions caused by thermal fluctuations at finite temperatures, we have plotted the magnon bands at three different temperatures, as shown in Fig. 5. The results revealed that, in addition to the renormalization of magnon energies, the gap at the \mathbf{K} point decreases with the

increase in temperature. When the temperature reaches a certain value, the gap closes, and further increases in temperature will reopen the gap. We have confirmed that all the topological phase transitions we observed occur with a magnetization greater than zero. This indicates that the topological transitions are stable and are not driven by the system reaching a state of zero magnetization.

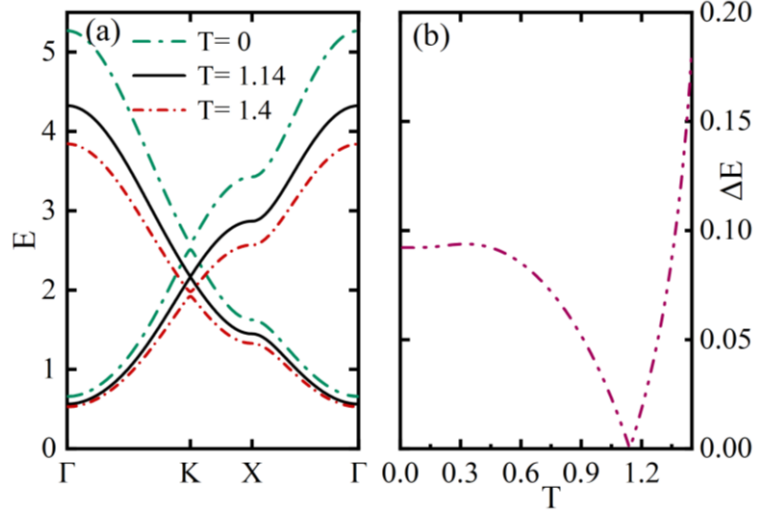


FIG. 5. Magnon band structures of the Kitaev-Heisenberg honeycomb ferromagnet for three different temperature along the path $\Gamma-K-M-\Gamma$. $D = 0.28$.

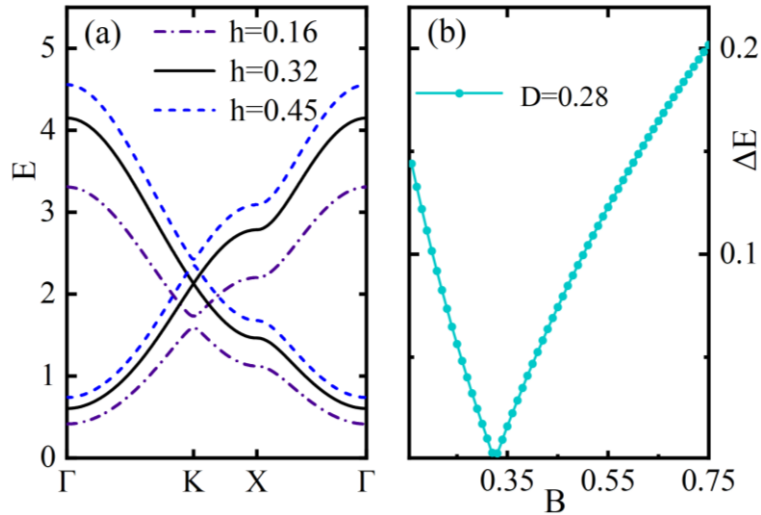


FIG. 6. Kitaev-Heisenberg honeycomb ferromagnet's band structure diagrams along the path $\Gamma-K-M-\Gamma$ at the same temperature. $D = 0.28$.

In our research, the time-reversal symmetry of the system is broken, which

allows us to use Chern numbers to quantify and characterize the topological properties of magnon bands, defined as $C_\lambda = \frac{1}{2\pi} \int_{BZ} d^2k B_\lambda^z(\mathbf{k})$, with Berry curvature $\mathbf{B}_\lambda(\mathbf{k}) = \nabla \times \mathbf{A}_\lambda$ and Berry connection $\mathbf{A}_\lambda = i \text{Tr}[\Gamma^\lambda \Lambda_{\mathbf{k}}^\dagger \boldsymbol{\tau}_z (\partial_{\mathbf{k}} \Lambda_{\mathbf{k}})]$, where Γ^λ is the diagonal matrix, taking a value of +1 for the λ mode and zero otherwise. A non-zero Berry curvature is the origin of the thermal Hall effect, which can serve as a signature of topological magnons, reflecting their geometric phase in momentum space. Topological phase transitions in magnons can alter the band structure and the Berry curvature, and these changes are manifested through thermal transport properties, particularly the thermal Hall effect. Thus, measuring the thermal Hall effect becomes a sensitive method for detecting these topological changes. The thermal Hall conductivity, a key parameter in examining the thermal Hall effect, is defined by the following equation:

$$k_{xy} = -\frac{k_B^2 T}{\hbar} \sum_{\lambda=\alpha,\beta} \int [d\mathbf{k}] B_\lambda^z(\mathbf{k}) c_2(n_{\mathbf{k},\lambda}) \quad (20)$$

Where $[d\mathbf{k}] = d^2\mathbf{k} / (2\pi)^2$, k_B^2 is the Boltzmann constant, \hbar is the reduced Planck constant, $c_2(x) = (1+x) \left(\ln \frac{1+x}{x} \right)^2 - (\ln x)^2 - 2\text{Li}_2(-x)$, $\text{Li}_2(-x)$ is the polylogarithm function.

We have plotted the temperature-dependent thermal Hall conductivities k_{xy} values with three different DMI for comparison. It can be observed that all k_{xy} exhibit discontinuous behavior and a sign reversal, which can be explained by the transition of Berry curvature near the \mathbf{K} point, where the band gap closes and reopens, and the Berry curvature experiences a jump from positive to negative values. From Eq. (20), it is evident that the thermal Hall conductivity is related to the distribution of Berry curvature and the occupation number of magnon bands. The discontinuous change in Berry curvature leads to the discontinuous behavior of k_{xy} at T_c , which is consistent with the discontinuity of Berry. Furthermore, we found that

the phase transition temperature increases with the value of DMI. Physically speaking, the sign reversal of the thermal Hall conductivity is an important indicator of a topological phase transition.

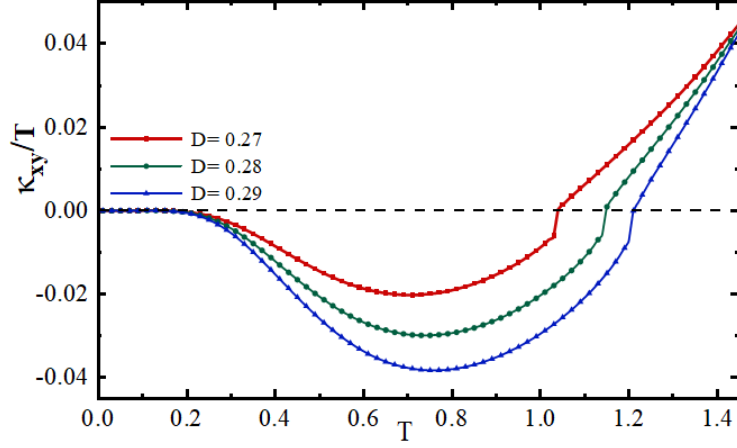


FIG.7. The thermal Hall conductivity of three different D . The corresponding critical temperature T_c is $T_c = 1.04, 1.15, 1.21$, respectively.

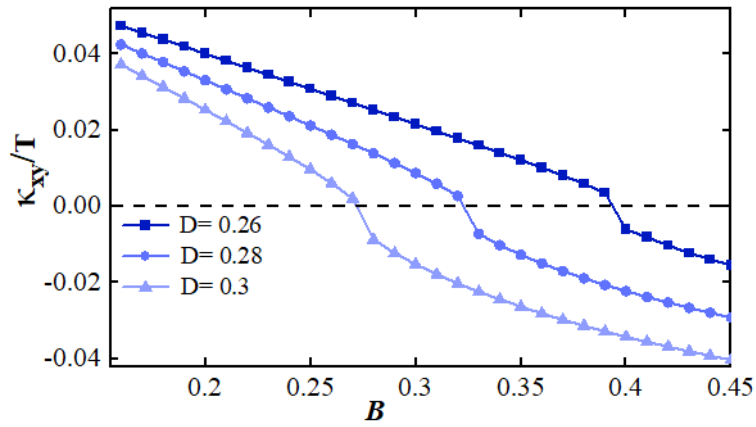


FIG. 8. Showing the relationship between the thermal Hall conductivity and magnetic field strength at the same temperature for three different DMI interactions was drawn. $T = 1.3$. The corresponding critical magnetic field $h_c = 0.39, 0.32, 0.28$, respectively.

In FIG. 8, we discuss three different magnitudes of DMI at the same temperature and plot k_{xy} as a function of magnetic field strength B . In conjunction with Fig.6, it can be clearly seen that as the field strength continuously increases, the energy gap closes and reopens. k_{xy} undergoes a distinct sign reversal with the increase of

B , and the larger the DMI, the easier it is to achieve a topological transition. The topological phase of the system can be tuned by temperature or external magnetic fields. The corresponding continuous topological phase transitions, driven by these magnon interactions, are accompanied by the phenomenon of gap closure. The sign of the thermal Hall conductivity directly reflects the Chern number, which characterizes the topological phase. Therefore, the sign reversal occurs during the topological phase transition and can serve as an indicator for future experiments. We note here that similar results were also reported in reference [30], where the non-conservation of particle number interactions is a key factor.

IV. CONCLUSION

This study investigates the effects of magnon-magnon interactions and thermal fluctuations on magnonic properties in Heisenberg-Kitaev honeycomb ferromagnets using the SCR spin wave theory at finite temperatures. The study focuses on systems with Kitaev and DMI interactions under the influence of Heisenberg exchange, magnetocrystalline anisotropy, and an external magnetic field. The results show that magnetization and topological phase transitions can be induced by temperature and field strength, with the external magnetic field enhancing magnetic anisotropy and increasing the Curie temperature. The paper is structured to establish the model and treat many-body interactions using finite-temperature field theory, and numerically solve self-consistent equations to calculate magnon bands and topological invariants at finite temperatures. The study also examines the thermal Hall effect as a manifestation of magnons' topological phase transitions, providing a comprehensive numerical analysis complementing the theoretical discussions.

Acknowledgments

J. Wang thanks Prof. B. Tang and Prof. Y.-M. Li for helpful discussions. This work was supported by the National Natural Science Foundation of China under Grant No. 12064011 and the College Students Innovation and Entrepreneurship Training Program of Hunan Province under Grant No. S202310531065.

References

- [1] N. P. Armitage, E. J. Mele, and A. Vishwanath, Weyl and Dirac semimetals in three-dimensional solids, *Rev. Mod. Phys.* 90, 015001 (2018).
- [2] B. A. Bernevig, T. L. Hughes, and S.-C. Zhang, Quantum spin hall effect and topological phase transition in HgTe quantum wells, *Science* 314, 1757 (2006).
- [3] I. Garate, Phonon-Induced Topological Transitions and Crossovers in Dirac Materials, *Phys. Rev. Lett.* 110, 046402 (2013).
- [4] D. Zhang, W. K. Lou, M. S. Miao, S. C. Zhang, and K. Chang, Interface-Induced Topological Insulator Transition in GaAs/Ge/GaAs Quantum Wells, *Phys. Rev. Lett.* 111, 156402 (2013).
- [5] M. S. Miao, Q. Yan, C. G. Van de Walle, W.-K. Lou, L. L. Li, and Kai Chang, Polarization-Driven Topological Insulator Transition in a GaN/InN/GaN Quantum Well, *Phys. Rev. Lett.* 109, 186803 (2012).
- [6] X.-L. Qi and S.-C. Zhang, Topological insulators and superconductors, *Rev. Mod. Phys.* 83, 1057 (2011).
- [7] L. Lu, J. D. Joannopoulos, and M. Soljačić, Topological photonics, *Nat. Photonics* 8, 821 (2014).
- [8] J. Lu, C. Qiu, L. Ye, X. Fan, M. Ke, F. Zhang, and Z. Liu, Observation of topological valley transport of sound in sonic crystals, *Nat. Phys.* 13, 369 (2017).
- [9] R. Shindou, R. Matsumoto, S. Murakami, and J. Ohe, Topological chiral magnonic edge mode in a magnonic crystal, *Phys. Rev. B* 87, 174427 (2013).
- [10] Y.-M. Li, J. Xiao, and K. Chang, Topological magnon modes in patterned ferrimagnetic insulator thin films, *Nano Lett.* 18, 3032 (2018).
- [11] Z. Hu, L. Fu, and L. Liu, Tunable Magnonic Chern Bands and Chiral Spin Currents in Magnetic Multilayers, *Phys. Rev. Lett.* 128, 217201 (2022).
- [12] S. K. Kim, H. Ochoa, R. Zarzuela, and Y. Tserkovnyak, Realization of the Haldane-Kane-Mele model in a system of localized spins, *Phys. Rev. Lett.* 117, 227201 (2016).
- [13] R. Chisnell, J. S. Helton, D. E. Freedman, D. K. Singh, R. I. Bewley, D. G. Nocera, and Y. S. Lee, Topological magnon bands in a kagome lattice ferromagnet, *Phys. Rev. Lett.* 115, 147201 (2015).
- [14] A. Mook, J. Henk, and I. Mertig, Edge states in topological magnon insulators, *Phys. Rev. B* 90, 024412 (2014).
- [15] L. Zhang, J. Ren, J.-S. Wang, and B. Li, Topological magnon insulator in insulating ferromagnet, *Phys. Rev. B* 87, 144101 (2013).
- [16] Y.-M. Li, Y.-J. Wu, X.-W. Luo, Y. Huang, and K. Chang, Higher-order topological phases of magnons protected by magnetic crystalline symmetries, *Phys. Rev. B* 106, 054403 (2022).
- [17] X. S. Wang, H. W. Zhang, and X. R. Wang, Topological magnonics: A paradigm for spin-wave manipulation and device design, *Phys. Rev. Appl.* 9, 024029 (2018).
- [18] H. Kondo and Y. Akagi, Dirac surface states in magnonic analogs of topological crystalline insulators, *Phys. Rev. Lett.* 127, 177201 (2021).
- [19] T. Hirokawa, S. A. Díaz, J. Klinovaja, and D. Loss, Magnonic quadrupole topological insulator in antiskyrmion crystals, *Phys. Rev. Lett.* 125, 207204 (2020).
- [20] A. Mook, K. Plekhanov, J. Klinovaja, and D. Loss, Interaction stabilized topological magnon Insulator in ferromagnets, *Phys. Rev. X* 11, 021061 (2021).
- [21] A. V. Chumak, V. I. Vasyuchka, A. A. Serga, and B. Hillebrands, Magnon spintronics, *Nat. Phys.* 11, 453 (2015).
- [22] V. Baltz, A. Manchon, M. Tsoi, T. Moriyama, T. Ono, and Y. Tserkovnyak, Antiferromagnetic

- spintronics, *Rev. Mod. Phys.* **90**, 015005 (2018).
- [23] B. Wei, J.-J. Zhu, Y. Song, and K. Chang, Renormalization of gapped magnon excitation in monolayer MnBi_2Te_4 by magnon-magnon interaction, *Phys. Rev. B* **104**, 174436 (2021).
- [24] T. Oguchi, Theory of spin-wave interactions in ferro- and antiferromagnetism, *Phys. Rev.* **117**, 117 (1960).
- [25] S. H. Liu, Nonlinear spin-wave theory for antiferromagnets, *Phys. Rev.* **142**, 267 (1966).
- [26] S. S. Pershoguba, S. Banerjee, J. C. Lashley, J. Park, H. Ågren, G. Aeppli, and A. V. Balatsky, Dirac magnons in honeycomb ferromagnets, *Phys. Rev. X* **8**, 011010 (2018).
- [27] Z. Li, T. Cao, and S. G. Louie, Two-dimensional ferromagnetism in few-layer van der Waals crystals: Renormalized spin-wave theory and calculations, *J. Magn. Magn. Mater.* **463**, 28 (2018).
- [28] B. Wei, J.-J. Zhu, Y. Song, and K. Chang, Renormalization of gapped magnon excitation in monolayer MnBi_2Te_4 by magnon-magnon interaction, *Phys. Rev. B* **104**, 174436 (2021).
- [29] F. J. Dyson, General theory of spin-wave interactions, *Phys. Rev.* **102**, 1217 (1956).
- [30] Heng. Z, H. C. Shi, Z. G. Tang, and B. Tang, Interacting topological magnons in a checkerboard ferromagnet. *Chin. Phys. B* **33**, 1045 (2024).
- [31] Koyama, S, Nasu, J. Thermal Hall effect incorporating magnon damping in localized spin systems. *Physical Review B* **109**, 17 (2024).
- [32] D. S. Maior, E. C. Souza, S. M. Rezende, Magnon energy renormalization in yttrium iron garnet, *Phys. Rev. B* **108**, 5 (2023).
- [33] L. Wojek, M. H. Berntsen, V. Jonsson, A. Szczerbakow, P. Dziawa, B. J. Kowalski, T. Story, O. Tjernberg, Direct observation and temperature control of the surface Dirac gap in a topological crystalline insulator, *Nat. Commun.* **6**, 8463 (2015).
- [34] V. V. Mkhitarian and L. Ke, Self-consistently renormalized spin-wave theory of layered ferromagnets on the honeycomb lattice, *Phys. Rev. B* **104**, 064435 (2021).
- [35] S. S. Pershoguba, S. Banerjee, J. C. Lashley, J. Park, H. Ågren, G. Aeppli, and A. V. Balatsky, Dirac magnons in honeycomb ferromagnets, *Phys. Rev. X* **8**, 011010 (2018).
- [36] A. Mook, K. Plekhanov, J. Klinovaja, and D. Loss, Interaction-stabilized topological magnon insulator in ferromagnets, *Phys. Rev. X* **11**, 021061 (2021).
- [37] H. Sun, D. Bhowmick, B. Yang, P. Sengupta, Interacting topological Dirac magnons, *Phys. Rev. B* **107**, 13 (2023).
- [38] Y.-S. Lu, J.-L. Li, and C.-T. Wu, Topological Phase Transitions of Dirac Magnons in Honeycomb Ferromagnets, *Phys. Rev. Lett* **127**, 217202 (2021).
- [39] Heng. Z, H. Shi, Z, B. Tang, Topological phase transitions in a honeycomb ferromagnet with unequal Dzyaloshinskii-Moriya interactions, *Eur. Phys. J. Plus* **138**, 11 (2023).
- [40] Heng. Z, H. Shi, Z, B. Tang, Interacting topological magnons in a checkerboard ferromagnet. *Chin. Phys. B* **33**, 3 (2024).
- [41] Y.-M. Li, W. Luo, K. Chang, Temperature-induced magnonic Chern insulator in collinear antiferromagnets, *Phys. Rev. B* **107**, 21 (2023).
- [42] S. Murakami and A. Okamoto, Thermal Hall Effect of Magnons, *J. Phys. Soc. Jpn.* **86**, 011010 (2017).
- [43] S. A. Owerre, Topological thermal Hall effect in frustrated kagome antiferromagnets, *Phys. Rev. B* **95**, 014422 (2017).
- [44] S. A. Owerre, Topological honeycomb magnon Hall effect: A calculation of thermal Hall conductivity of magnetic spin excitations, *J. Appl. Phys.* **120**(4), 043903 (2016).

- [45] A. Mook, S. A. Díaz, J. Klinovaja, and D. Loss, Chiral hinge magnons in second-order topological magnon insulators, *Phys. Rev. B* 104, 024406 (2021).
- [46] Z. Li, T. Cao, S.G. Louie, Two-dimensional ferromagnetism in few-layer van der Waals crystals: Renormalized spin-wave theory and calculations, *J. Magn. Magn. Mater.* 463, 28 (2018).
- [47] D. G. Joshi, Topological excitations in the ferromagnetic Kitaev-Heisenberg model. *Phys. Rev. B* 98, 6 (2018).
- [48] Li-Chuan Zhang, Fengfeng Zhu, Dongwook Go, Fabian R. Lux, Flaviano Jos´e dos Santos, Samir Lounis, Yixi Su, Stefan Blügel, and Yuriy Mokrousov, “Interplay of Dzyaloshinskii-Moriya and Kitaev interactions for magnonic properties of Heisenberg-Kitaev honeycomb ferromagnets,” *Phys. Rev. B* 103, 134414 (2021).